Analysis of TEM image of quantum cascade laser heterostructure grown by metalorganic vapour-phase epitaxy

© An.A. Afonenko[1], A.A. Afonenko[1,¶], D.V. Usahkov[1], T.A. Bagaev[2], M.A. Ladugin[2], A.A. Marmalyuk[2], S.S. Pushkarev[3,4], R.A. Khabibullin[3,4]

[1] Belarusian State University,
220030 Minsk, Republic of Belarus
[2] „Polyus“ Research Institute of M.F. Stelmakh Joint Stock Company,
117342 Moscow, Russia
[3] Institute of Ultrahigh Frequency Semiconductor Electronics, Russian Academy of Sciences,
117105 Moscow, Russia
[4] Moscow Institute of Physics and Technology,
141701 Dolgoprudnyi, Russia

¶ E-mail: afonenko@bsu.by

Received April 15, 2024
Revised June 20, 2024
Accepted June 20, 2024

The transmission electron microscopy (TEM) image of a quantum cascade heterostructure was analyzed. A heterostructure containing 185 periods and four quantum wells GaAs/$Al_{0.15}Ga_{0.85}As$ in each period was grown by MOVPE. Different composition spreading laws (normal, exponential and asymmetric exponential) have been used to reveal the differences in the composition deviation at the interface „barrier/quantum well“ and „quantum well/barrier“ when interpolating the experimental hetero-interface profile. The effect of finite sample thickness on the composition fluctuation characteristics has been theoretically investigated and spectra and autocorrelation functions of composition fluctuations have been obtained. Estimates of the thickness of hetero-interface roughness and its correlation length have been carried out.

Keywords: quantum cascade laser, transmission electron microscopy, hetero-interface, GaAs, AlGaAs.

DOI: 10.61011/SC.2024.04.58844.6256H

1. Introduction

The study aimed at analyzing the structural perfection of grown samples is an important stage in the development of the technology for growing quantum cascade laser heterostructures [1]. The information about the thicknesses and compositions of semiconductor layers is the most valuable, which is necessary for predicting the characteristics of lasers and validating the constitutive parameters and theoretical models used. The information about the thickness of the transition layers and the characteristics of the roughness of the interfaces is necessary to account for the spectral broadening of energy levels and the correct calculation of the gain spectra [2–4].

The hetero-interface roughness scattering (IRS) was calculated in the approximation of the coherent potential in Ref. [5] and their effect on the tunneling current through the two-barrier structure of GaAs−A1GaAs was experimentally confirmed. A significant contribution of IRS to the width of the intersubband absorption line in the quantum well (QW) is shown in Ref. [6,7], along with optical phonon scattering. The effect of IRS on both current and gain in terahertz quantum cascade lasers (THz QCL) was studied in Ref. [2,8,9]. The simulation shows that IRS causes leakage currents for laser levels and can significantly reduce the gain. The improvement of epitaxial growth technology, optimization of band designs and minimization of IRS resulted in a significant increase of maximum operating temperatures of THz QCL [9–14] from $T_{max} \sim 200$ K in 2012 [10] to $T_{max} = 261$ K in 2023 [14].

The results of the analysis of the TEM image of the quantum cascade heterostructure $Al_{0.15}Ga_{0.85}As$/GaAs epitaxially grown by the interaction of organometallic compounds and hydrides (MOVPE) [15] are presented in this paper with a resolution of 0.226 nm per pixel; the sizes of the transition regions, the root-mean-square roughness of the hetero interfaces and their autocorrelation functions are found. The design of the metalorganic vapour-phase epitaxy quantum cascade heterostructure is based on the two-photon emission scheme proposed and described in Ref. [16,17].

2. Analysis of the heterostructure profile

The pixel intensity of the TEM image was summed along the inclined lines marked in Figure 1 for restoring the profile of the hetero-interfaces in the studied heterostructure. The optimal slope was chosen from the condition of maximum contrast of the resulting profile. The profile sampling interval was 0.19 nm taking into account the image slope. Three types of composition spreading functions were used to fit the reconstructed profile using the least squares method (Figure 2):
normal —

$$f_g(z) = \exp\left(-\frac{z^2}{2\tau_g^2}\right), \quad (1)$$

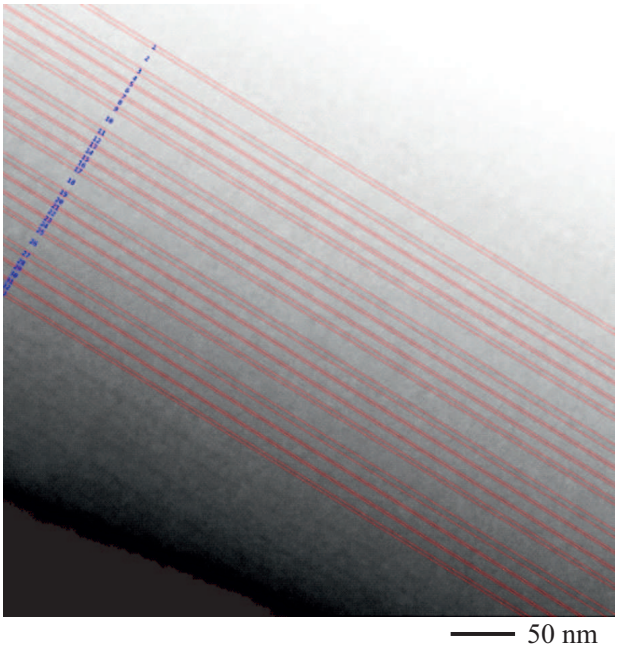

Figure 1. TEM image of the QCL heterostructure region with marked layers after processing of the profile and revealing the interfaces of GaAs quantum wells and AlGaAs barriers.

symmetric exponential —

$$f_e(z) = \frac{1}{\exp\left(-\frac{\pi}{2}\frac{z}{\tau_e}\right) + \exp\left(-\frac{\pi}{2}\frac{z}{\tau_e}\right)}, \qquad (2)$$

asymmetric exponential —

$$f_{ab}(z) = \frac{1}{\exp\left(-\frac{\pi}{2}\frac{z}{\tau_a}\right) + \exp\left(-\frac{\pi}{2}\frac{z}{\tau_b}\right)}. \qquad (3)$$

Here τ_g, τ_e, τ_a, τ_b — the root-mean-square values of spreading for the corresponding functions.

The intensity of the TEM image has a significant background gradient as can be seen from Figure 2. The Fourier transform [1] is not suitable for analyzing the composition profile due to the background gradient. Polynomials of various degrees were used to subtract the background. The completed calculations showed that the recoverable layer thicknesses depend on the order of the polynomial used to subtract the background (see Table 1). The order of the polynomial should be at least the number of analyzed periods for individual selection of the background level for each period of the heterostructure (we analyzed 4 periods of the structure). The maximum value of the polynomial order is approximately limited by the number of barriers or quantum wells (17 layers in our case). The background will have a component that replicates the profile of the structure with higher values of the order of the polynomial, as a result of which subtraction of the background will lead to a decrease of the amplitude of the restored profile. The interpolation order at which the amplitude of the restored profile A is maximal can be considered as the best. The best n values of the order of background interpolation for normal interface broadening are in the range of 7–10 in the considered example. The restored thicknesses turned out to be the same for these values. The largest range of thickness variation for different background interpolation orders was 0.34 nm. The restored value of the hetero-interfaces broadening of 1.13–1.17 nm is less sensitive to the order of the polynomial (spread 3%).

Similar results are obtained when using other composition spreading functions. The best interpolation order depends on the type of function (see Table 2). The maximum spread of the recoverable thicknesses was 0.15 nm, which does not exceed one step of image sampling. The smallest discrepancy value is obtained for normal interface broadening with a given background interpolation order.

The root-mean-square hetero-interface broadening for the asymmetric exponential profile was $\tau_a = 1.37$ nm,

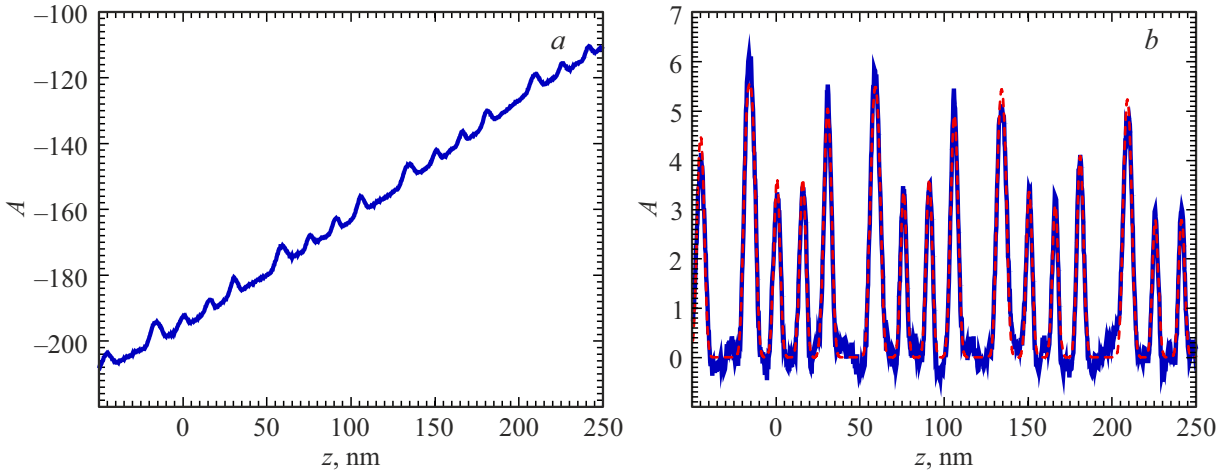

Figure 2. *a* — dependence of the row average pixel intensity A of the processed TEM image on the coordinate z directed along the normal to the plane of the layers from the upper right corner of the TEM image; *b* — composition profile, restored using the normal composition spreading function at the 7th order of background interpolation.

Table 1. The restored amplitude of the profile A, hetero-interface broadening τ and structure layer thicknesses d averaged over 4 periods and heterostructure period D for normal distribution for different orders of n interpolation of the background (maximum and minimum values are in bold font)

n	A, rel. un.	τ nm	d, nm								D, nm
4	5.66	1.15	3.27	16.63	4.71	8.65	**1.7**8	**9.52**	1.78	8.36	54.69
5	5.64	1.14	3.22	16.63	4.76	8.65	**1.78**	**9.52**	**1.73**	8.36	54.64
6	5.61	1.14	**3.08**	16.58	4.90	8.51	1.83	**9.52**	1.78	**8.41**	54.59
7–10	**5.72**	**1.17**	3.12	**16.72**	**4.66**	**8.70**	1.87	9.32	1.87	8.31	54.59
11	5.41	**1.13**	3.36	**16.48**	**4.95**	**8.41**	**2.02**	9.23	1.97	8.22	54.64
12	5.54	1.16	**3.41**	16.63	4.66	8.65	1.97	**9.18**	**2.02**	**8.17**	54.69
Max	5.72	1.17	3.41	16.72	4.95	8.70	2.02	9.52	2.02	8.41	54.69
Min	5.41	1.13	3.08	16.48	4.66	8.41	1.78	9.18	1.73	8.17	54.59
Max–Min	0.31	0.04	0.33	0.24	0.29	0.29	0.24	0.34	0.29	0.24	0.10

Table 2. The restored amplitude of the profile A, hetero-interface broadening τ and the thickness of the layers of the structure averaged over 4 periods d and the period of the heterostructure D for different blur functions

Broadening	n	A, rel. units	τ, nm	d, nm								D, nm
Normal	7	5.72	1.17	3.12	16.72	4.66	8.70	1.87	9.32	1.87	8.31	54.59
Exponential	10	6.04	1.42	3.08	16.77	4.66	8.70	1.87	9.32	1.87	8.31	54.59
Asymmetrical exponential	6	6.06	1.37/1.44	3.03	16.77	4.66	8.65	1.83	9.42	1.78	8.46	54.59

$\tau_b = 1.44$ nm. Therefore, no significant differences of the profile of the heterojunctions „quantum well/barrier“ and „barrier/quantum well“ as well as the structures grown by molecular beam epitaxy were revealed [18].

It should be noted that the resolution of the TEM image, equal to 0.226 nm per pixel, was obtained from the result of X-ray analysis, according to which the period is 54.7 nm. Therefore, all the found thicknesses provided in the Tables 1 and 2, for which the period is not equal to the specified one, should be proportionally scaled which is a common practice in analyzing TEM images [1].

3. Effect of sample thickness on fluctuation autocorrelation function

The composition of the heterostructure, determined by the analysis of TEM images, is an average value over the sample thickness L. The autocorrelation function of fluctuations of the measured values in the TEM image is represented as

$$K_{\mathrm{TEM}}(\Delta x) = \left\langle \frac{1}{L}\int_0^L f(x,y)dy \cdot \frac{1}{L}\int_0^L f(x-\Delta x,y)dy \right\rangle = \frac{1}{L^2}\int_0^L\int_0^L \langle f(x,y)\cdot f(x-\Delta x,y')\rangle dy\,dy', \quad (4)$$

where $f(x,y) = f(\mathbf{r})$ — fluctuation of the composition in the plane of the layer. The y-axis direction is selected here in the direction of the path of the TEM rays. The autocorrelation function of fluctuations of measured values can be found from the following integral in the isotropic approximation of the fluctuation autocorrelation function $K(\Delta r) = \langle f(\mathbf{r})\cdot f(\mathbf{r}-\Delta\mathbf{r})\rangle$

$$K_{\mathrm{TEM}}(\Delta x) = \frac{1}{L^2}\int_0^L\int_0^L K\left(\sqrt{\Delta x^2 + (y'-y)^2}\right)dy\,dy'. \quad (5)$$

The Gaussian form is most often used as approximations for the fluctuation autocorrelation function

$$K(x) = \sigma_x^2 \exp\left(-\frac{x^2}{L_c^2}\right) \quad (6)$$

or an exponential form

$$K(x) = \sigma_x^2 \exp\left(-\frac{|x|}{L_c}\right), \quad (7)$$

where L_c — correlation length, σ_x — standard deviation.

The measured root-mean-square value of the fluctuations in the TEM image decreases with the increase of the sample thickness (Figure 3). For large sample thicknesses, it is

$$\sigma_{x\mathrm{TEM}} = \sqrt{K_{\mathrm{TEM}}(0)} \approx \sigma_x\sqrt{2L_c/L}. \quad (8)$$

The functional form of the Gaussian autocorrelation function (6) and the correlation length does not change in case of averaging (5). The functional form after averaging (5) can be represented by a similar exponential function (7)

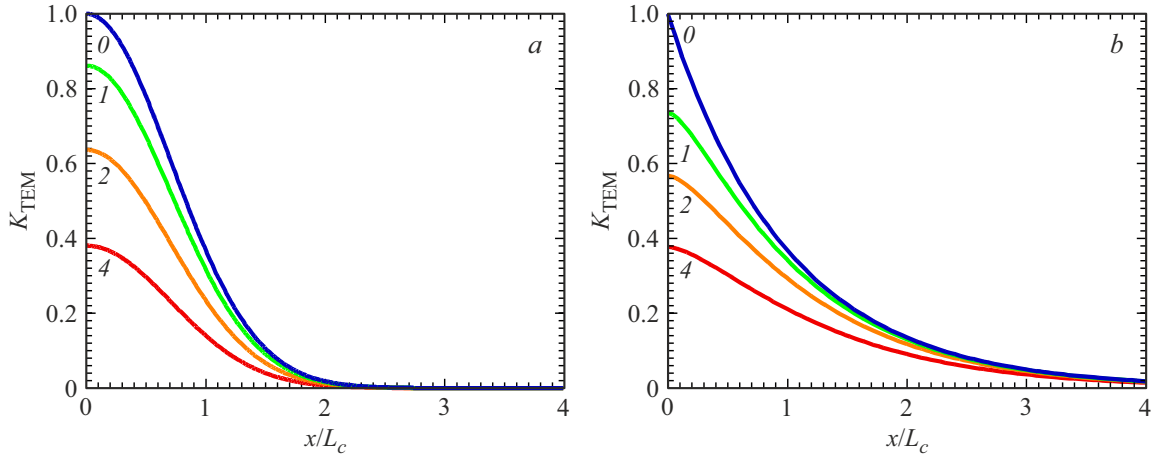

Figure 3. Dependence of the normalized autocorrelation function of the sample for Gaussian (a) and exponential (b) correlation of fluctuations with different ratios of sample thickness L and correlation length L_c: $L/L_c = 0, 1, 2, 4$. (The colored version of the figure is available on-line).

only approximately for the exponential autocorrelation function (7). For finding the effective correlation length $L_{c\mathrm{TEM}}$, we take into account that the Fourier transform of the correlation function on the plane is used in the calculation of scattering. The most significant are the Fourier components for small wave vectors. Therefore, it is advisable to use the following expression for an effective correlation length

$$L^2_{c\mathrm{TEM}} = \int_0^\infty r K_{\mathrm{TEM}}(r)dr / K_{\mathrm{TEM}}(0), \qquad (9)$$

which ensures the equality of the zero Fourier component for the exact function (5) and an approximate function of the form (7). As the thickness of the sample increases, the measured correlation length of the exponential correlation function tends to

$$L_{\mathrm{TEM}} = \sqrt{2}L_c. \qquad (10)$$

4. Analysis of fluctuations in the component composition of the heterostructure

The brightness differs significantly in different parts of the image (see Figure 1), therefore, it is necessary to exclude background illumination for the analysis of fluctuations. Subtraction of the background using a polynomial (as was done in the first section of the article) is unacceptable for these purposes, since it is not local and results in the distortion of the correlation dependence. Image elements can be combined only in the direction of the normal to the layers for ensuring locality. For this purpose we assume that only the composition x of barrier layers $Al_xGa_{1-x}As$ can fluctuate, since the material should be close to a GaAs binary semiconductor in wide quantum wells, i. e., we will consider the intensity of the image within the quantum wells as the background. Let us divide the entire image into stripes for subtracting the background, the boundaries of these stripes pass through the middle of the quantum wells according to the previously reconstructed structure profile. Each stripe is divided crosswise into sections with a thickness of one pixel. A linear regression is found for each such section of the stripe using the least squares method for the intensity of the image, which is consider to be the background. Only those pixels are taken into account for calculating the regression coefficients for the background that are within the region of quantum wells according to the previously restored structure profile. Next, the resulting regression (background) is substracted from the intensity of the image of the entire section of the stripe, including the barrier area (Figure 4).

The concept of hetero-interface roughness is usually used in the analysis of scattering. Let's assume that the hetero-interface region falls within the range $\pm\tau$ from the selected interface according to the previously restored structure profile (τ — root-mean-square hetero-interface broadening). Let us average the fluctuations of the image perpendicular to the layers in the range $\pm\tau$ and obtain a one-dimensional dependence of the composition along the hetero-interface. The root-mean-square value of fluctuations in the composition of the hetero-interface σ_x can be converted to the equivalent roughness of the barrier layer

$$\sigma_d = 2\tau\frac{\sigma_x}{x_b}, \qquad (11)$$

where x_b — the average composition of the barrier layer. Alternatively, it is possible to average the fluctuations of the image perpendicular to the layers in the entire barrier layer and obtain characteristics of fluctuations in the heterocomposition of the barrier layer.

The average spectral density of the fluctuation is almost constant for wave numbers $k \geq 3\,\mathrm{nm}^{-1}$ for the analyzed image (see Figure 4) (Figure 5), which suggests the presence of white noise in the TEM image. Let us take into account

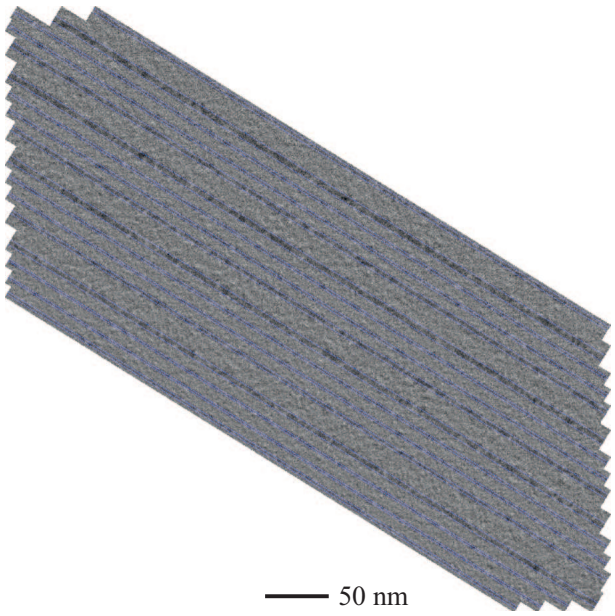

Figure 4. Processed TEM image with marked layers after subtracting the background in the analyzed region.

for estimating the correlation length L_c that half of the „energy“ of fluctuations for normal (6) and exponential (7) correlation function is within the range of wave numbers $k < 0.95/L_c$ and $k < 1/L_c$, respectively. Only the low-frequency part of the spectrum $k < 3\,\text{nm}^{-1}$ is taken into account for calculating the „energy“ of fluctuations from which white noise is subtracted based on its average level in the high-frequency region. The value of the correlation length was 2.4 nm, the relative root-mean-square fluctuation of the barrier composition was 28%, the root-mean-square roughness of the hetero-interfaces was 0.65 nm.

The spatial autocorrelation functions of fluctuations of the heterocomposition obtained by the Fourier transform of their spectral density have a decreasing form (Figure 5), which can be approximately described by the exponential function (7). In this case, the dependencies before and after the white noise subtraction differ markedly only in the value at the origin. It should be noted that the fluctuation spectra and spatial autocorrelation functions obtained by averaging the fluctuation spectra for periodic boundary conditions and averaging autocorrelation functions without periodic boundary conditions practically do not differ.

Taking into account ratios (8) and (10) and assuming the sample thickness of $L = 30\,\text{nm}$, we find that the length of the roughness correlation is $L_c = 1.7\,\text{nm}$, and the root mean square roughness of the hetero-interfaces is 1.9 nm for interpolation of the correlation function by the exponential dependence. The obtained roughness of the hetero-interfaces is an order of magnitude higher than the values from the literature data [6]. This may suggest that fluctuations in the intensity of the analyzed TEM image are more due to roughness or contamination of the sample surface.

5. Conclusion

A technique for analyzing the profile and roughness of hetero-interfaces based on TEM images of the heterostructure of a quantum cascade laser grown by the MOVPE method is demonstrated in the paper. A TEM image of the quantum cascade heterostructure $Al_{0.15}Ga_{0.85}As/GaAs$ with a resolution of 0.226 nm per pixel was analyzed. The calculated sizes of the transition regions in the heterostructure were 1.2 and 1.4 nm, in case of interpolation of the interface broadening with a normal and exponential distribution, respectively. There were no significant differences in the profile of the „barrier/quantum well“ and „quantum well/barrier“ heterojunctions. The layer thicknesses reconstructed by the least squares method have a maximum spread of 0.34 nm, depending on the degree of the polynomial for background interpolation and the spreading function. The best agreement of experimental and

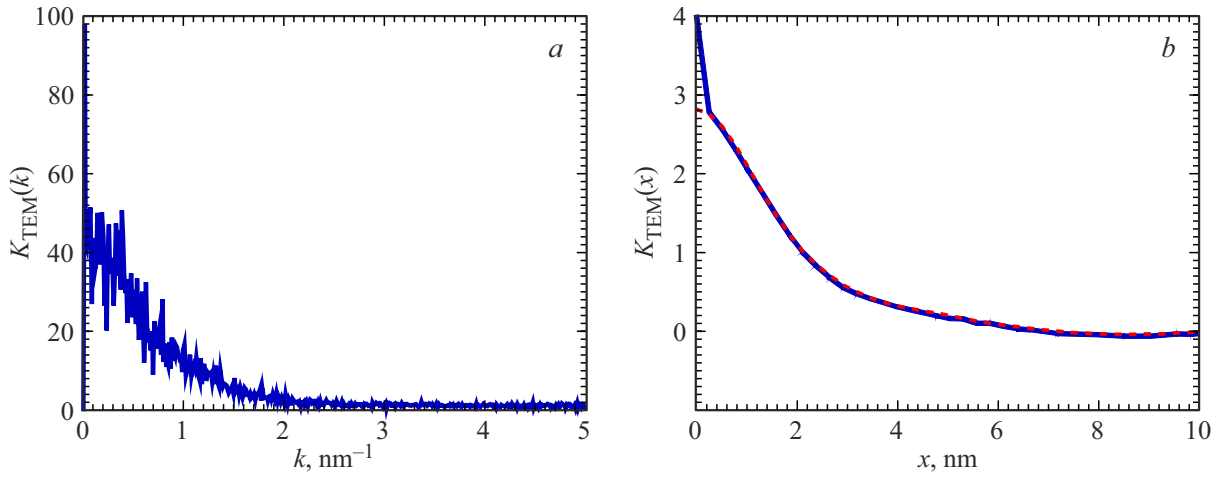

Figure 5. (a) The spectral density averaged over all analyzed hetero-interfaces and (b) autocorrelation function of composition fluctuation before (blue line) and after subtraction of white noise (red line).

calculated profiles is obtained for the interface broadening according to the normal law. The estimated correlation length of the roughness of the hetero-interfaces was 1.7 nm, the root-mean-square deviation was 1.9 nm, which suggests a significant contribution of roughness or contamination of the sample surface to fluctuations of the intensity of the analyzed TEM image.

Funding

The study was supported financially within the scope of the projects of Belarusian Republican Foundation for Basic Research F23RNFM-064 and by the grant from the Russian Science Foundation No. 24-49-10004, https://rscf.ru/project/24-49-10004/.

Conflict of interest

The authors declare that they have no conflict of interest.

References

[1] X. Lü, E. Luna, L. Schrottke, K. Biermann, H.T. Grahn. Appl. Phys. Lett., **113** (17), 172101 (2018).
[2] Y.V. Flores, A. Albo. IEEE J. Quant. Electron., **53** (3), 2300208 (2017).
[3] D.V. Ushakov, A.A. Afonenko, A.A. Dubinov, V.I. Gavrilenko, O.Yu. Volkov, N.V. Shchavruk, D.S. Ponomarev, R.A. Khabibullin. Kvant. elektron., **49**(10), 913 (2019). (in Russian).
[4] A.E. Yachmenev, S.S. Pushkarev, R.R. Reznik, R.A. Khabibullin, D.S. Ponomarev. Progr. Cryst. Growth and Characterization Mater., **66** (2), 100485 (2020).
[5] P. Johansson. Phys. Rev. B, **46** (19), 12865 (1992).
[6] T. Unuma, T. Takahashi, T. Noda, M. Yoshita, H. Sakaki, M. Baba, H. Akiyama. Appl. Phys. Lett., **78** (22), 3448 (2001).
[7] T. Unuma, M. Yoshita, T. Noda, H. Sakaki, H. Akiyama. J. Appl. Phys., **93** (3), 1586 (2003).
[8] K.A. Krivas, D. O. Winge, M. Franckié, A. Wacker. J. Appl. Phys., **118**, 114501 (2015).
[9] M. Franckié, D.O. Winge, J. Wolf, V. Liverini, E. Dupont, V. Trinité, J. Faist, A. Wacker. Opt. Express, **23** (4), 5201 (2015).
[10] S. Fathololoumi, E. Dupont, C.W.I. Chan, Z.R. Wasilewski, S.R. Laframboise, D. Ban, A. Mátyás, C. Jirauschek, Q. Hu, H.C. Liu. Opt. Express, **20** (4), 3866 (2012).
[11] R.A. Khabibullin, K.V. Maremyanin, D.S. Ponomarev, R.R. Galiev, A.A. Zaitsev, A.I. Danilov, I.S. Vasilevsky, A.N. Vinichenko, A.N. Klochkov, A.A. Afonenko, D.V. Ushakov, S.V. Morozov, V.I. Gavrilenko. FTP, **55** (11), 989 (2021). (in Russian).
[12] L. Bosco, M. Franckié, G. Scalari, M. Beck, A. Wacker, J. Faist. Appl. Phys. Lett., **115**, 010601 (2019).
[13] A. Khalatpour, A. K. Paulsen, C. Deimert, Z.R. Wasilewski, Q. Hu. Nature Photonics, **15**, 16 (2021).
[14] A. Khalatpour, A. Tam, S.J. Addamane, Z. Wasilewski, Q. Hu. Appl. Phys. Lett., **122**, 161101 (2023).
[15] T.A. Bagaev, M.A. Ladugin, A.A. Marmalyuk, A.I. Danilov, D.V. Ushakov, A.A. Afonenko, A.A. Zaitsev, K.V. Maremyanin, S.V. Morozov, V.I. Gavrilenko, R.R. Galiev, A.Yu. Pavlov, S.S. Pushkarev, D.S. Ponomarev, R.A. Khabibullin. Pis'ma ZhTF, **48** (10), 16 (2022). (in Russian).
[16] D.V. Ushakov, A.A. Afonenko, R.A. Khabibullin, V.K. Kononenko, I.S. Manak. *Vestsi Natsyianal'nai akademii navuk Belarusi. Seryia fizika-matematychnykh navuk*. Proc. National Academy of Sciences of Belarus. Ser. Phys. Mathematics, **58** (2), 237 (2022).
[17] D.V. Ushakov, A.A. Afonenko, D.S. Ponomarev, S.S. Pushkarev, V.I. Gavrilenko, R.A. Khabibullin. Izv. vuzov. Radiofizika, LXV, № 5-6, 505 (2022). (in Russian).
[18] An.A. Afonenko, A.A. Afonenko, D.V. Ushakov, S.S. Pushkarev, R.A. Khabibullin. *Tr. XXV Mezhd. simp. „Nanofizika i nanoelektronika“ (N. Novgorod)*, **2**, s. 566 (2021). (in Russian).

Translated by A.Akhtyamov